Applied Radiation and Isotopes 83 (2014) 57–67

Contents lists available at ScienceDirect

Applied Radiation and Isotopes

journal homepage: www.elsevier.com/locate/apradiso

Electron scattering cross section calculations for polar molecules over a broad energy range

A.G. Sanz [a], M.C. Fuss [a], F. Blanco [b], Zdeněk Mašín [c], Jimena D. Gorfinkiel [c], F. Carelli [d], F. Sebastianelli [d], F.A. Gianturco [d], G. García [a,e,*]

[a] Instituto de Física Fundamental, Consejo Superior de Investigaciones Científicas, Serrano 113-bis, 28006 Madrid, Spain
[b] Departamento de Física Atómica, Molecular y Nuclear, Universidad Complutense de Madrid, Ciudad Universitaria, 28040 Madrid, Spain
[c] Department of Physical Sciences, The Open University, Walton Hall, Milton Keynes, MK7 6AA, United Kingdom
[d] Department of Chemistry, "Sapienza" University of Rome, P.le A. Moro 5, 00185 Rome, Italy
[e] Centre for Medical Radiation Physics, University of Wollongong, NSW 2522, Australia

HIGHLIGHTS

- Integral and differential cross sections have been calculated for HCN and pyrimidine.
- ePOLYSCAT and *R*-matrix were joined together with IAM-SCAR at intermediate energies.
- Complete sets of integral cross sections are provided over a broad energy range.
- The Dickinson correction is confirmed to improve the large angles differential cross sections for strong polar molecules.

ARTICLE INFO

Available online 31 January 2013

Keywords:
Pyrimidine
HCN
Electron scattering
Elastic cross sections
Dipole-induced excitations

ABSTRACT

We report computational integral and differential cross sections for electron scattering by two different polar molecules, HCN and pyrimidine, over a broad energy range. We employ, for low energies, either the single-centre expansion (ePOLYSCAT) or the *R*-matrix method, while for the higher energies we select a corrected form of the independent-atom representation (IAM-SCAR). We provide complete sets of integral electron scattering cross sections from low energies up to 10,000 eV. Our present calculated data agree well with prior experimental results.

1. Introduction

Single-track structure simulations are a useful tool for modelling radiation-induced damage in biological matter (Agostinelli et al., 2003; Baró et al., 1995), which underpins numerous applications within the field of radiotherapy (Fuller et al., 2004; Gemmel et al., 2008) or radiodiagnosis. These models require interaction probabilities over a very broad energy range and for all the possible scattering processes energetically allowed. When any kind of primary radiation interacts with matter, around 80% of the energy is transferred via ionization to the media, while the remainder generates electronic and vibrational excitations (Märk et al., 1995). Large quantities of secondary species are therefore produced, among which secondary electrons (SEs) with energies below 30 eV are the most abundant, being generated with a yield of 4×10^4/MeV of deposited radiation (Pimblott and LaVerne, 2007). The importance of the role played by the electrons with low energies (LEEs) is clearly recognized: at subionization or even subexcitation energies they have the ability to induce single- and double-strand breaks in the DNA molecule. This suggests that in order to achieve good therapeutic outcomes, databases for track simulations require complete sets of electron scattering cross sections, from high energies down to the very low energies of thermalised secondary electrons.

Numerous biologically relevant molecules also have a considerably high permanent dipole moment, starting with the water molecule H_2O (Suresh and Naik, 2000), DNA/RNA bases (Kulakowski et al., 1974; DeVoe and Tinoco, 1962; Weber and Craven, 1990) and THF (Nelson et al., 1967). Polar targets, however, normally bring additional difficulties both for experimental and theoretical studies. First of all, the excitation energy of the rotational levels is so small that the energy resolution of the experiments is not enough to distinguish these inelastic processes from the elastic events. Additionally, the angular distribution of the scattered electrons from a polar molecule is strongly peaked

* Corresponding author at: Instituto de Física Fundamental, Consejo Superior de Investigaciones Científicas, Serrano 113-bis, 28006 Madrid, Spain.
Tel.: +34 91 5616800-943214.
E-mail address: g.garcia@iff.csic.es (G. García).

0969-8043/$ - see front matter © 2013 Elsevier Ltd. All rights reserved.
http://dx.doi.org/10.1016/j.apradiso.2013.01.031

in the forward direction however, the angular resolution of the experiments is not enough to distinguish the elastically scattered electrons from the unscattered ones. On the other hand, electron scattering calculations with polar molecules are more delicate than with non-polar targets. The long-range nature of the dipole potential implies that large number of partial waves (angular momenta) have to be considered in the wave function expansion and that rotational motion should be taken into account since its neglect leads to divergences in the cross sections at low energies, as is always the case when treating the collision processes within the body-fixed frame of reference.

As a computational test for such types of molecules, we have performed calculations involving two different polar molecules, hydrogen cyanide, HCN, and pyrimidine, $C_4H_4N_2$. HCN is indeed a rather simple polyatomic molecule and therefore appropriate for checking computational models of dipole excitations. In contrast, pyrimidine is a more complex molecule which is normally used as a model molecule to study electron scattering from DNA bases. Three of the DNA/RNA bases: cytosine, thymine and uracil are pyrimidine derivatives. Their low-symmetry and electron-rich structure make the more symmetric pyrimidine computationally preferable as an initial benchmark for the present study.

Electron collisions with HCN have been studied in numerous occasions with special attention given to identifying the paths for dissociative electron attachment (DEA) channels (Burrow et al., 1992; May et al., 2010; Varambhia and Tennyson, 2007; Chourou and Orel, 2009). Computational studies focused on determining interaction probabilities (cross sections) are fairly scarce. Measurements of elastic cross sections have been provided by Srivastava et al. (1978) at electron impact energies from 3 up to 50 eV. Theoretical cross sections, including electronically inelastic cross sections, have been calculated within a restricted energy range by Faure et al. (2007) and Jain and Norcross (1985), at low energies, and by Jain and Baluja (1992) at high energies. It is only recently that a complete set of integral electron cross sections covering a wide energy range have been provided by us (Sanz et al., 2012). Electron collisions with pyrimidine are also of broad interest so it has therefore been subject of numerous studies including the measurement of elastic differential cross sections both in the low energy range 3–50 eV (Palihawadana et al., 2011) and for higher impact energies ranging from 50 to 300 eV (Maljković et al., 2009). In the former work, electronically inelastic cross sections were also measured within the same energy range. Vibrational and electronic excitation cross sections have been experimentally provided by Levesque et al. (2005) in the condensed phase. Electron energy-loss measurements for gaseous pyrimidine in the energy range between 2 and 15 eV have been reported by Ferreira da Silva et al. (2010). Theoretical elastic cross sections were calculated at low energies by means of the Schwinger multichannel technique (Palihawadana et al., 2011) and more recently, Mašín et al. (2012) determined both elastic and electronically inelastic cross sections by means of the *R*-matrix method (Burke, 2011). For higher energies, elastic and electronically inelastic (electronic excitation and ionization) integral cross sections, together with the elastic-scattering angular distributions, have been calculated by the Madrid's group using the IAM-SCAR method (Maljković et al., 2009; Palihawadana et al., 2011).

As the above summary suggests, studies of electron collisions involving polar biomolecules have been restricted to a small energy range and therefore cross sectional data for the different scattering processes covering a very broad energy range is still lacking. That is why, in the present work, we propose a computational approach by means of combining different quantum scattering models which are known to be accurate over different energy regions. Hence, we shall employ the symmetry adapted-single centre expansion (SA-SCE) approach known as ePOLYSCAT (Gianturco et al., 1994; Natalense and Lucchese, 1999) and the *R*-matrix (Burke, 2011) method at low energies, while at higher incident energies a corrected form of the independent-atom model (IAM), i.e., the screening-corrected additivity rule IAM-SCAR (Blanco and García 2003b, 2004) method shall be used. Using these methodologies we are able to provide complete sets of integral elastic, electronically inelastic and total electron cross sections (CS) over a very broad energy range for molecules possessing a substantial permanent dipole moment.

Section 2 briefly summarizes the scattering methods we have employed: ePOLYSCAT, *R*-matrix and IAM-SCAR, together with their respective approaches to the calculation of rotational excitations. Section 3 presents the details of our calculations and shows our cross sections, together with a discussion of the present results. Finally, our work is summarized in Section 4 and some concluding remarks are also presented.

2. Theoretical methods

2.1. The low energy region

The *ab-initio* molecular quantum mechanical methods we employ to study the electron-molecule interaction at low incident energies have been thoroughly discussed in previous works (Baccarelli et al., 2008; Gianturco and Lucchese 2004; Burke, 2011; Tennyson, 2010), hence we only present here a brief summary. In both the symmetry adapted-single centre expansion (SA-SCE) and the *R*-matrix methods the target nuclei are kept fixed at their ground state equilibrium geometry.

Within the SA-SCE method the total wave function of the $(N+1)$ electrons is represented as an antisymmetrized product of Hartree–Fock orbitals of the neutral ground-state molecular target; during the whole scattering process, the N bound electrons are considered to be in the ground electronic state of the target at its optimized nuclear geometry. This means that the scattering process is limited to the elastic channels and no electronic excitations are considered. Then, to obtain the scattering equations, the potentials and any arbitrary three-dimensional function describing either one of the N bound electrons or the scattered electronic particle, are expanded in a set of symmetry adapted angular functions around the centre of mass and over a numerical radial grid out of the asymptotic region. We further assume that the electron-molecule interaction potential is described by a model local potential, which is comprised of three different terms: the static V^{st}, the exchange V^{ex} and the correlation-polarization potential V^{CP}. The static term is given by the attractive interaction between the scattering electron and the positive nuclei plus the local part of the repulsive interaction with the target electrons. The initial exact nonlocal exchange potential is replaced by an energy-dependent local function of the electron density of the target by employing the Free Electron Gas Exchange (FEGE) potential described by Hara (1967). And finally, the dynamical response of the target to the impinging electron, that is the correlation and polarization effects acting at short and long-range, respectively, is described by the energy-independent Lee–Yang–Parr (Lee et al., 1998) correlation potential which is matched to the long-range dipole polarizibility term at a certain r_{match}, as given in detail by Lucchese and Gianturco (1996). These approximations lead to the following coupled partial equations for the $(N+1)$th electron in the single centre expansion (SCE) representation:

$$\left[\frac{d^2}{dr^2}-\frac{l(l+1)}{r^2}+k^2\right]f_{lh}^{p\mu}(r)=2\sum_{l'h'}V_{lh,\,l'h'}^{p\mu}(r)f_{l'h'}^{p\mu}(r) \tag{1}$$

where the indexes l, h represent the "angular channel" and the potential coupling elements are given by:

$$V^{p\mu}_{lh,\,l'h'}(r) = X^{p\mu}_{hl}(\hat{r})|V(r)|X^{p\mu}_{h'l'}(\hat{r}) = \int d\hat{r} X^{p\mu}_{hl}(\hat{r})V(r)X^{p\mu}_{h'l'}(\hat{r}). \quad (2)$$

In summary, for each collision energy the numerical solutions of the coupled Eq. (1) produce the relevant K-matrix elements, from which the differential and integral elastic cross sections are derived using the above theoretical tools implemented in the ePOLYSCAT code (Gianturco et al., 1994; Natalense and Lucchese, 1999) specifically designed for this purpose.

The R-matrix method is based on dividing the coordinate space of the electron-molecule collision problem into an inner and outer region, separated by a sphere of radius $r=a$ centred at the centre of mass of the molecule. This sphere must be sufficiently large to enclose the whole electronic density of the target states included in the calculation. The interaction between the scattering electron and the target is differently described in each region. Inside the R-matrix sphere the short-range interactions between the scattering electron and the N bound target electrons, exchange and electron–electron correlation, are described accurately; the scattering wave function of the $N+1$ electron system is therefore expressed as a close-coupling (CC) expansion:

$$\psi^{N+1}_k = \mathrm{A}\sum_{i,j} a_{ijk}\phi_i(x_1 \ldots x_N)u_{ij}(x_{N+1}) + \sum_i b_{ik}\chi_i(x_1 \ldots x_{N+1}) \quad (3)$$

where k represents the kth solution of the $N+1$ Hamiltonian in the inner region, **A** is the antisymmetrization operator, $u_{ij}(x_i)$ are the continuum orbitals describing the scattering electron and x_i are the spatial and spin coordinates of electron i, a_{ijk} and b_{ik} are variational coefficients, ϕ_i are electronic target wave functions and χ_i, built as products of target molecular orbitals (occupied and virtual), are known as L^2-functions and are crucial for the representation of the short-range polarization and correlation effects. Note that the wave functions from Eq. (3) do not depend on the kinetic energy of the scattering electron and are therefore calculated only once, a feature that provides a substantial advantage in terms of computational requirements. In the outer region ($r>a$) the exchange and correlation effects are negligible and a long-range multipolar expansion can be used to represent the electron-target interaction. In order to obtain scattering information, a set of coupled differential equations describing the behaviour of the scattering electron must be solved. For that, the R-matrix is built at the boundary between the regions using the inner region information and then is propagated up to a radius large enough so that an asymptotic expansion for the radial wave functions can be matched to known analytical asymptotic solutions. The corresponding K-matrices containing the scattering information are determined, and subsequently integral and differential cross sections are produced via the generation of the necessary T-matrices.

The R-matrix calculations have been performed at different levels of approximation using the UKRmol suite (Carr et al., 2012). The simplest scattering method that we have employed is the static exchange plus polarization (SEP) model, in which the target wave function is described at the Hartree–Fock level considering just the ground state of the molecule. The correlation and polarization effects are included through the L^2 configurations, where one electron from the valence space of the target is allowed to be promoted to one of a selected number of virtual orbitals, which are also available for the scattering electron. Additionally, we have used a more sophisticated model that is known as the close-coupling (CC) approximation in which, apart from the ground state of the target, a number of excited target electronic states are included in the CC expansion (28 in our calculations). The target wave functions are calculated at the complete active space self-consistent field (CASSCF) level. The CC method allows us determine electronic excitation cross sections.

It is important to note at this point that both the R-matrix and the ePOLYSCAT methods have been described within the fixed nuclei approximation (FNA), which considers the time scale of the impinging electron to be short compared to the nuclear motions so that the nuclei are treated as fixed particles during the collision process. This approximation is correctly justified for molecules with no permanent dipole moment. However, in the case of electron scattering with polar targets where the interaction potential includes long-range multipolar terms, the FNA treatment is known to cause divergences in the elastic DCS, especially in the forward direction caused by the lack of convergence in the partial-wave expansion for large l (Norcross and Collins, 1982). This divergence can be only removed by the introduction of the nuclear motion in the Hamiltonian (Collins and Norcross, 1978) leading, in principle, to more complicated coupled equations (Lane, 1980). Alternatively, this divergence can also be avoided in a more convenient way by using the first Born approximation (FBA) for the point-dipole potential, that permits us to calculate analytically the contributions from all the partial waves, both individually and as summed quantities (Crawford, 1967). In accordance with this approximation, a variety of Born top-up procedures have been developed during the last years as described in detailed by Zhang et al. (2009). Among them, we have chosen the frame-transformation POLYDCS method, implemented by Sanna and Gianturco (1998). Although still an approximate approach, the POLYDCS implementation has been demonstrated to generate reliable state-to-state rotationally elastic and inelastic cross sections for numerous biomolecules of arbitrary geometry. Within this approach, after allowing rotational motion by applying a frame transformation from the body-fixed (BF) to the space-fixed (SF) frame of reference, slow convergence of the partial-wave expansion is circumvented by determining the differential cross sections (DCS) using:

$$\frac{d\sigma}{d\Omega} = \frac{d\sigma^B}{d\Omega} + \sum_L \left(A_L - A_L^B\right) P_L(\cos(\theta)) \quad (4)$$

The above expression basically indicates that partial cross sections for low partial waves up to l_{max} are calculated *ab-initio*, in our case, either the UKR-mol or ePOLYSCAT suites so that short-range effects are considered, while higher partial waves are introduced by calculating the total cross section using the Born approximation and then subtracting the partial cross sections for the low-partial waves already considered ($l<l_{max}$). Hence, the formula given by Eq. (4) can be understood as a short-range correction to the original Born approximation (Sanna and Gianturco 1998). Moreover, the present cross sections were calculated from the ground rotational state ($j=0$) of the molecule, i.e., independent of the temperature of the experiment, since Okamoto et al. (1993) demonstrated that the elastic DCS does not depend on the initial rotational state unless the scattering angle is very close to 0°. For our calculations we have included transitions up to $j=3$ and $j=4$ for HCN and pyrimidine, respectively.

2.2. The high energy region

In the high energy region we apply the well-known corrected form of the independent-atom model IAM-SCAR (screening-corrected additivity rule). Details for this procedure have also been extensively described in previous works (Blanco and García 2002, 2003a, 2003b, 2004) hence, only a brief summary of it is given here. Contrary to the aforementioned low-energy electron scattering methods, IAM-SCAR does not consider anymore the molecule as a single target, but instead, as an aggregate of atoms that

are believed to scatter independently by assuming that the molecular binding does not affect the electronic distribution of the atom. Thus, the first concern of this calculation is the interaction probabilities for the constituent atoms, namely, C, H and N. Each atomic target is described by a complex optical potential, whose real part accounts for the elastic scattering of the incident electrons while the imaginary part represents the inelastic processes which are considered as 'absorption' channels from the incident beam. This complex potential for each atom has the following form:

$$V_{\mathrm{opt}}(r) = V_R(r) + iV_{\mathrm{abs}}(r) = V_s(r) + V_{\mathrm{ex}}(r) + V_{\mathrm{pol}}(r) + iV_{\mathrm{abs}}(r) \qquad (5)$$

where the real part comprises three terms: (i) the static term derived from a Hartree–Fock calculation of the atomic charge distribution (Cowan, 1981), (ii) an exchange term to account for the indistinguishability of the incident and target electrons which is given by the semiclassical energy-dependent formula derived by Riley and Truhlar (1975), and (iii) a polarization potential for the long-range interactions which depend on the target dipole polarizibility, in the form given by Zhang et al. (1992). Finally, the absorption potential accounts for the electronically inelastic scattering events. It is based on the Staszewska's quasifree model (Staszewska et al., 1983) but incorporates some improvements to the original formulation, such as the inclusion of screening effects, local velocity corrections and the description of the electron's indistinguishability (Blanco and García 2002), leading therefore to a model which provides a realistic approximation for electron–atom scattering over a broad energy range. A recent excellent example of this can be seen in Zatsarinny et al. (2011) where our IAM-SCAR elastic results for the atomic target iodine (I) were in very good agreement with the cross sections computed using the more sophisticated Dirac-B-spline *R*-matrix method.

As a second step, molecular cross sections are computed from the atomic data by applying a coherent addition, commonly known as the additivity rule (AR). This procedure gives reasonable results for energies above 100 eV, as the incident electrons are fast enough to effectively "see" the target molecule as a sum of individual atoms. For lower energies, the atomic cross sections are sufficiently large to overlap, leading to an overestimation of the cross sections calculated with the additivity rule. This limitation has been resolved by introducing some screening coefficients which modify both differential and integral cross sections, as implemented in the SCAR code by Blanco and García (2003b, 2004). This method has been proved to be a powerful tool to calculate electron scattering cross sections, albeit only down to intermediate energies (down to about 30 eV), for a large variety of nonpolar molecules (Limão-Vieira et al., 2005, 2011; Kato et al., 2012).

From the previous description we can infer that both vibrational and rotational excitations are ignored in the IAM-SCAR method. However, in the case of polar targets, dipole-induced rotational excitations are not negligible and must be included in the scattering calculations. The method we follow in this case, based on the one suggested by Jain (1988), assumes the interaction of a charged particle with a free electric dipole in the framework of the first Born approximation (FBA). Then the calculated differential and integral rotational excitation cross sections are incorporated within our IAM-SCAR calculation in an incoherent way, i.e., by adding the results as a channel independent from the other channels. Although rotational excitation energies are, in general, fairly small (typically a few meV) in comparison with the incident electron energies, in order for the FBA to be valid, the latter energies should be higher than about 20 eV. Under these circumstances, rotational excitation cross sections are calculated by weighting the population for the *j*th rotational quantum level at 300 K and estimating the average excitation energy from the corresponding rotational constants. The complete approach, called the IAM-SCARD method, has been shown to be successful when applied to some polar molecules (Muñoz et al., 2007; Zecca et al., 2011). However, when the target molecule has a strong permanent dipole moment, as is the case of many biomolecules, it is known that the FBA fails for medium and large scattering angles. In order to partially solve this problem, we introduced a correction based on that suggested by Dickinson (1977), which brings a substantial improvement (Sanz et al., 2012) to the calculated cross sections. This procedure introduces a first-order corrective term to the differential cross sections for medium and large angles but maintains the FBA correction for lower angles:

$$\frac{d\sigma^{B}}{d\Omega} \approx \frac{D^2}{6E_i}\frac{1}{\sin^2(\theta/2)} \quad \theta < \theta_c \qquad (6)$$

$$\frac{d\sigma^{Dck}}{d\Omega} \approx \frac{\pi D}{64E_i}\frac{1}{\sin^3(\theta/2)} \theta < \theta_c \qquad (7)$$

where D is the permanent dipole moment of the molecule and E_i the energy of the projectile. Provided the dipole moment is larger than $D=0.75$ D, both curves smoothly join together at a specific critical angle θ_c where they cross each other.

3. Results and discussion

3.1. Details of the calculation

In the low energy range the cross sections have been computed either with the ePOLYSCAT or the *R*-matrix models for hydrogen cyanide and pyrimidine, respectively. In the case of HCN, the initial target wave function was generated by the Gaussian suite of codes (Frisch et al., 2004) at the Hartree–Fock level and using the 6-311++G (3df, 3pd) basis set. These *ab-initio* calculations yielded for the neutral molecule an equilibrium geometry in fairly good agreement with the experiments (Herzberg, 1966). The bound and scattering wave functions were expanded around the centre-of-mass of the target including partial waves up to $l_{max}=30$ and the multipolar expansion of the potential included terms up to $\lambda_{max}=60$. The range of integration has been tested for convergence, finally using a radial box size of 11.5 Å, and the discrete (r,θ,φ) grid of the scattered wave function involved a total of $1464\times84\times324$ points. HCN belongs to the $C_{2\infty}$ point group and has a very strong dipole moment: the experimental value is 2.98 D (DeLeon and Muenter, 1984) while the computed dipole moment from our ground state wave function turned to be 3.26 D. Further details about the calculations can be found in Sanz et al. (2012). Details of the *R*-matrix optimization tests performed for pyrimidine molecule are described in Mašín et al. (2012). Following this work, we have employed a compact basis set, cc-pVDZ generated both Hartree–Fock SCF and state-averaged CASSCF orbitals using MOLPRO (Werner et al., 2009), for the SEP and CC calculation, respectively. For the CASSCF calculations, an active space (10,8) was employed. Based on the experience gained in a previous work with the structural isomer pyrazine (Mašín and Gorfinkiel, 2011), the number of virtual orbitals was chosen to be 35–40 for the SEP and CC calculation, respectively. The scattered electron was described by a set of continuum orbitals built using a Gaussian-type orbitals (GTOs) basis set developed by Faure et al. (2002) which includes partial waves up to $l=4$. In order to guarantee that the electronic density of all the target states included in the calculation is negligible outside the *R*-matrix sphere, we have used a radius $a=13a_o$. Pyrimidine belongs to the C_{2v} point group and, although not as strong as the hydrogen cyanide molecule, it

also possess a significant permanent dipole moment: 2.31 D and 2.36 D, for the SEP and CC model, respectively, which can be compared with the experimental value of 2.334 D (Blackman et al., 1970). The best *R*-matrix results are obtained by combining two different levels of approximation: for energies below the first excitation threshold, which for pyrimidine is around 4 eV (Fischer et al., 2003), we use the SEP model, since it allows for a better representation of the short-range polarization and correlation effects. Above this limit, we use the CC model, which can describe electronic excitations and is therefore more realistic for describing this energy region.

For higher incident electron energies, integral cross sections for both hydrogen cyanide and pyrimidine have been computed by employing the IAM-SCAR model. The corresponding atomic cross sections for C, H and N have been previously calculated and discussed (Blanco and García, 2003a and references therein). Molecular cross sections have been calculated according to the available optimized geometrical parameters for HCN (Herzberg, 1966) and pyrimidine (Schreiber et al., 2008).

3.2. Elastic cross sections

Calculated elastic differential cross sections for HCN and pyrimidine are plotted in Figs. 1 and 2, respectively. A detailed analysis of Fig. 1, shows that at low energies the ePOLYSCAT-POLYDCS (dashed red line) angular distribution agrees qualitatively with the experimental data provided by Srivastava et al. (1978; green asterisk). Also, we find fair agreement with the calculations generated by Jain and Norcross (1985; solid-crossed brown line), although at 11.6 eV incident energy, some divergences seem to arise at the largest angles. At higher energies, as expected, the IAM-SCAR (solid blue line) method shows good agreement with the measurements, in particular at 50 eV, where the theoretical data lies within the experimental error bars. However, when rotation excitations are included (IAM-SCARD; dotted blue line) our data overestimates to some extent the experimental results at medium and large angles. As already discussed in the previous section, the Born approximation is known to fail from medium angles up to 180° whenever the permanent dipole moment of the target molecule is very large, as is the case of HCN. The Dickinson correction (dashed-dotted blue line) partially amends this failure and provides a more realistic representation at medium and large angles (for further details see Sanz et al. (2012)). In the case of pyrimidine (Fig. 2), in the low energy region, the agreement is very good between the *R*-matrix-POLYDCS (dashed red line) differential cross sections and the experimental data provided by Palihawadana et al. (2011) (green asterisk) for energies up to 15 eV, as has been shown in Mašín et al. (2012). In addition, there is good agreement with the Schwinger multichannel calculation (Palihawadana et al., 2011; dotted blue line), in particular at the lowest energies. In this energy range, the IAM-SCARD (dashed blue line) angular distribution curves are clearly larger in absolute value and present some differences in shape compared to the experiment. However, as the energy increases up to 50 eV, the independent-atom model comes into better agreement at medium and large angles with the experimental data from Palihawadana et al. (2011) and earlier results measured by Maljković et al. (2009). Indeed, there is excellent agreement throughout the whole angular range with the measurements from the Belgrade group (Maljković et al., 2009; brown triangles), starting at 100 eV and up to higher energies (not shown).

Integral elastic cross sections for HCN and pyrimidine are shown in Figs. 3 and 4, respectively. In Fig. 3 we present the integral elastic cross sections calculated at low energies with the single centre expansion method ePOLYSCAT (solid red line) and for high energies with the IAM-SCAR model (solid blue line), as described earlier. Note that that at intermediate energies both methods differ by around 50%. The origin of this discrepancy is attributed to the omission of the absorption term in the potential used by the ePOLYSCAT approach, since it has been proved that ignoring inelastic processes leads to an overestimation of the integral elastic CS, especially at energies above the ionization potential (Blanco and García, 2003a; Sanz et al., 2012). In other words, the single centre expansion method generates reliable elastic cross sections for energies below the ionization threshold, which for HCN is at 13.6 eV. On the other hand, when looking at the integral elastic cross sections for pyrimidine we find excellent agreement between the low-energy *R*-matrix results (solid red line) and the IAM-SCAR model (solid blue line) at intermediate energies, as can be seen in Fig. 4. As mentioned in the introduction, experiments do not, in general, have enough energy resolution ($E_r \sim 50$ meV) to distinguish the inelastic rotational excitations ($E_{rot} \sim 5$ meV) cross sections from the elastic cross sections. Therefore, in order to compare more realistically the calculated integral cross sections with the experimental data, we must include the rotational excitations in our elastic cross sections calculations. For HCN (Fig. 3), the elastic cross sections plus rotations are given by the ePOLYSCAT-POLYDCS approach (red dashed line) at low energies, and by the IAM-SCARD method at higher energies (blue dashed-dotted line). We now find fair agreement between both calculations, and also with the theoretical data computed by Faure et al. (2007) by means of the *R*-matrix method. Equivalent calculations were performed for pyrimidine (Fig. 4), but in this case, the *R*-matrix-POLYDCS approach (red dashed line) was used in the low energy range, attaining excellent agreement at intermediate energies with the high energy model discussed in the previous section.

In contrast with the fair agreement obtained between experiment and theory for the elastic angular distributions (Figs. 1 and 2), we observe marked discrepancies between the integral cross sections, specially at low energies (Figs. 3 and 4). It should be understood that, whereas the theoretical integral elastic CS plus rotational excitations correspond to integrating the differential cross sections from 0° to 180°, the integral experimental values have been obtained by extrapolating both for low and high angles since elastic DCS cannot be determined experimentally for the whole angular range. Hence, when both experimental and theoretical DCS are partially integrated only within the angular range where the experiments are able to measure the agreement is much better, as we have shown in previous works (Mašín et al., 2012, Sanz et al., 2012). This means that it is the extrapolation applied which induces the discrepancies in the integral cross sections. Moreover, since dipole-induced excitations are specially large at low angles, where experiments have no access, integral cross sections obtained from the experimental data are very sensitive to the extrapolation method applied when the target is a polar molecule.

3.3. Inelastic and total cross sections

Electronically inelastic and total cross sections are plotted for HCN and pyrimidine in Figs. 5 and 6, respectively. In the high energy region, electronically inelastic cross sections (electronic excitations and ionization), were calculated through the $iV_a(r)$ absorption term of the IAM-SCAR potential (Figs. 5 and 6, solid blue line) for energies above 10 eV. It should be noted that the electronic excitation threshold is normally placed at energies below 10 eV: 4.0 and 6.15 eV for pyrimidine (Fischer et al., 2003) and HCN (Nayak et al., 2005), respectively. However due to limitations of the present independent-atom model in the low-energy region, electronic excited states lying below 10 eV are ignored. For low energies, electronically inelastic cross sections were calculated for pyrimidine with the *R*-matrix close-coupling expansion method (Fig. 6, solid red line) including 28 excited

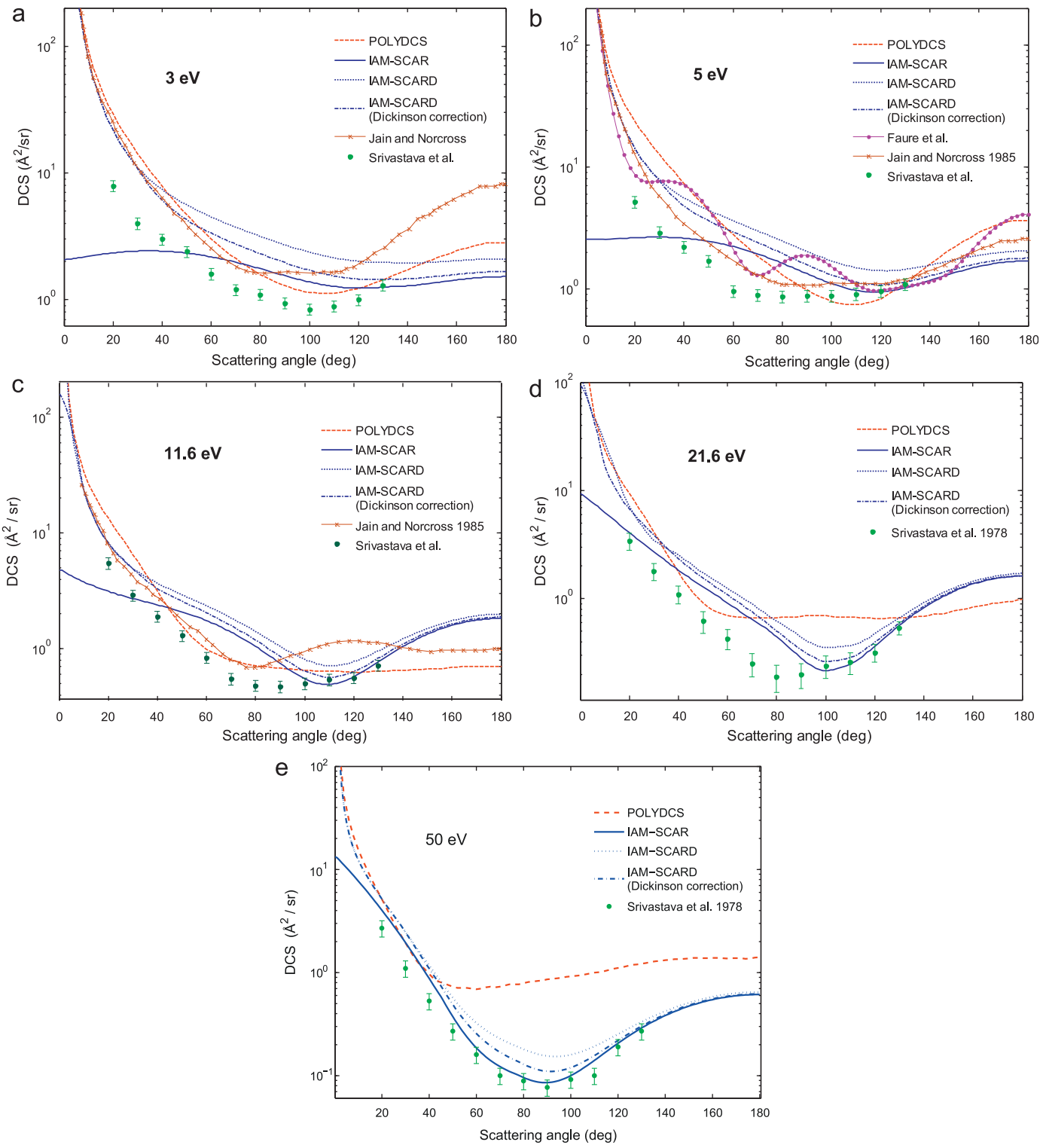

Fig. 1. Angular differential cross sections for elastic electron scattering from HCN for the incident energies indicated in the panels. Fig. 1a–e: (dashed red line) POLYDCS elastic differential cross sections; (solid blue line) IAM-SCAR elastic differential cross sections; IAM-SCARD elastic differential cross sections plus rotational excitations standard (dotted blue line) and with Dickinson correction (dashed-dotted blue line); (solid-crossed brown line) Jain and Norcross (1985) ESEP model; (solid-dotted purple line) Faure et al. (2007) *R*-matrix method calculation; (green asterisk) Srivastava et al. (1978) experimental data. (For interpretation of the references to colour in this figure legend, the reader is referred to the web version of this article.)

states (Mašín et al., 2012). However, ionized states of the target were not included in the CC expansion, and therefore the computed inelastic CS refers only to electronic excitations cross sections, consequently leading to a loss of accuracy for energies above the ionization threshold (9.7 eV in pyrimidine (Hush and Cheung, 1975)). Experimental results in the condensed phase from Levesque et al. (2005) for energies up to 10 eV, are in excellent agreement with the theoretical CC prediction. At 15 eV, there is good agreement between the experimental values presented in Mašín et al. (2012) obtained from electron energy loss spectra and the theoretical electronically inelastic cross sections computed by IAM-SCAR. These theoretical inelastic

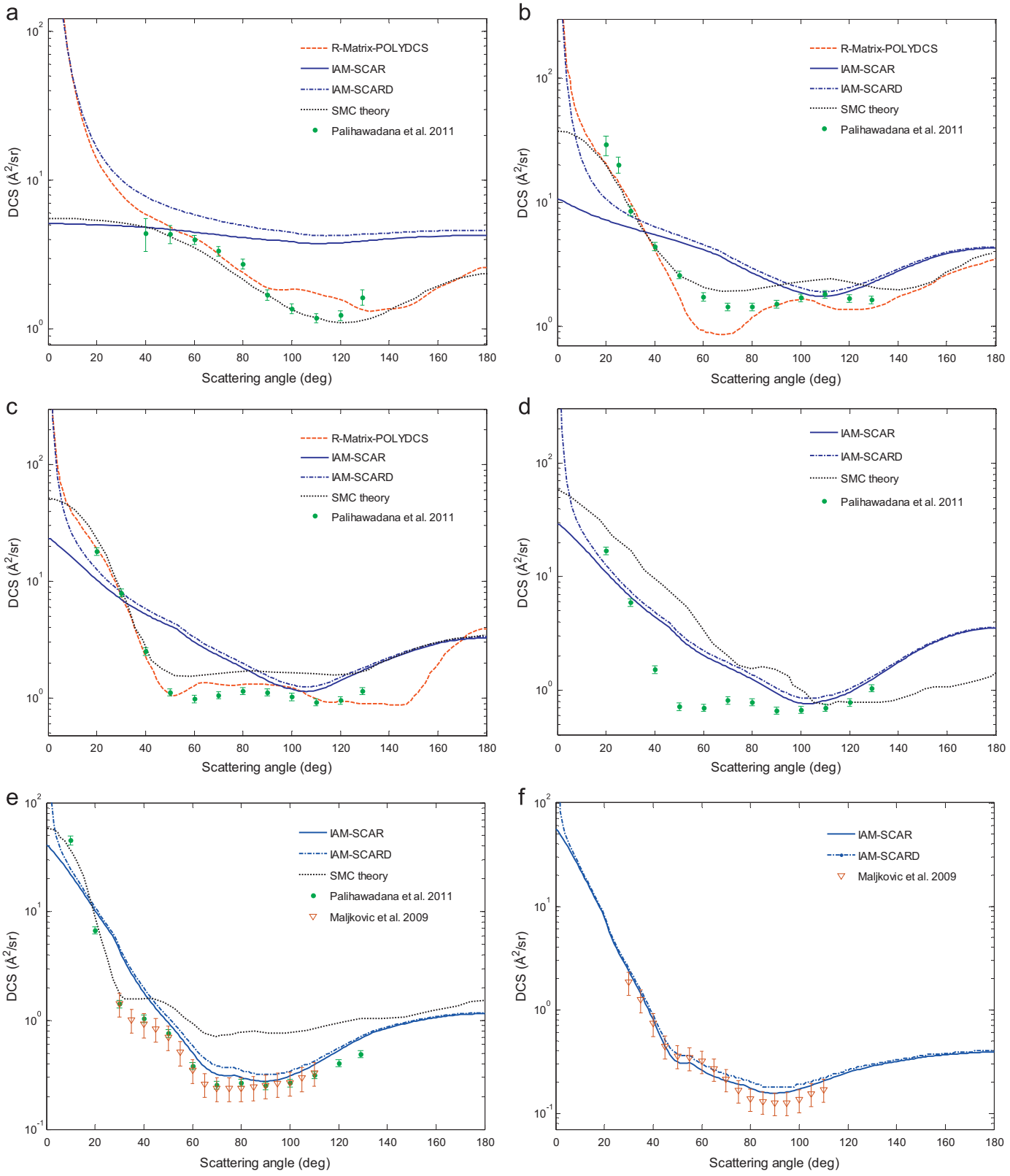

Fig. 2. Angular differential cross sections for elastic electron scattering from pyrimidine for the incident energies indicated in the panels. Fig. 1a–f: (dashed red line) *R*-matrix-POLYDCS elastic differential cross sections; (solid blue line) IAM-SCAR elastic differential cross sections; (dashed-dotted blue line) IAM-SCARD elastic differential cross sections plus rotational excitations; (dotted black line) Schwinger multichannel technique (Palihawadana et al., 2011); (green asterisk) Palihawadana et al. (2011) experimental data; (brown triangles) Maljković et al. (2009) experimental data. (a) 3 eV, (b) 10 eV, (c) 15 eV, d) 20 eV, (e) 50 eV and (f) 100 eV. (For interpretation of the references to colour in this figure legend, the reader is referred to the web version of this article.)

CS from IAM-SCAR procedure include both electronic excitation and ionization processes, while the experimental "total" inelastic CS accounts only for the electronic excitations. At higher energies above the ionization threshold ($E > 15$ eV), this leads to large differences in absolute values, although experimental and theoretical results show a similar trend with increasing energies. On

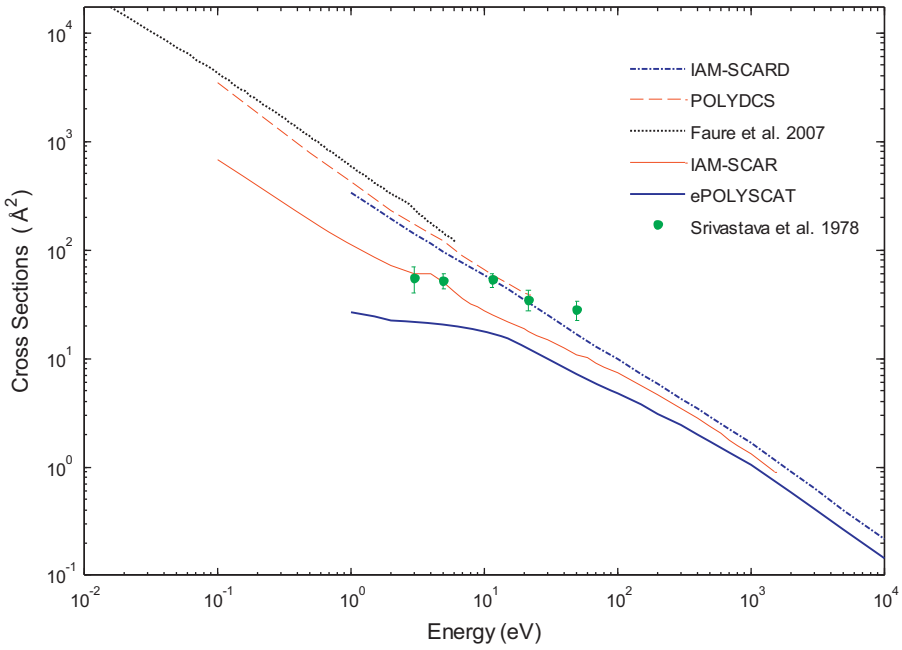

Fig. 3. Theoretical integral cross section for electron scattering by HCN: (solid red line) ePOLYSCAT elastic cross sections; (solid blue line) IAM-SCAR elastic cross sections; (dashed red line) POLYDCS elastic CS plus rotational excitations; (dashed-dotted blue line) IAM-SCARD elastic CS plus rotational excitations; (dotted black line) Faure et al. (2007) *R*-matrix method calculation; (green asterisk) Srivastava et al. (1978) experimental data. (For interpretation of the references to colour in this figure legend, the reader is referred to the web version of this article.)

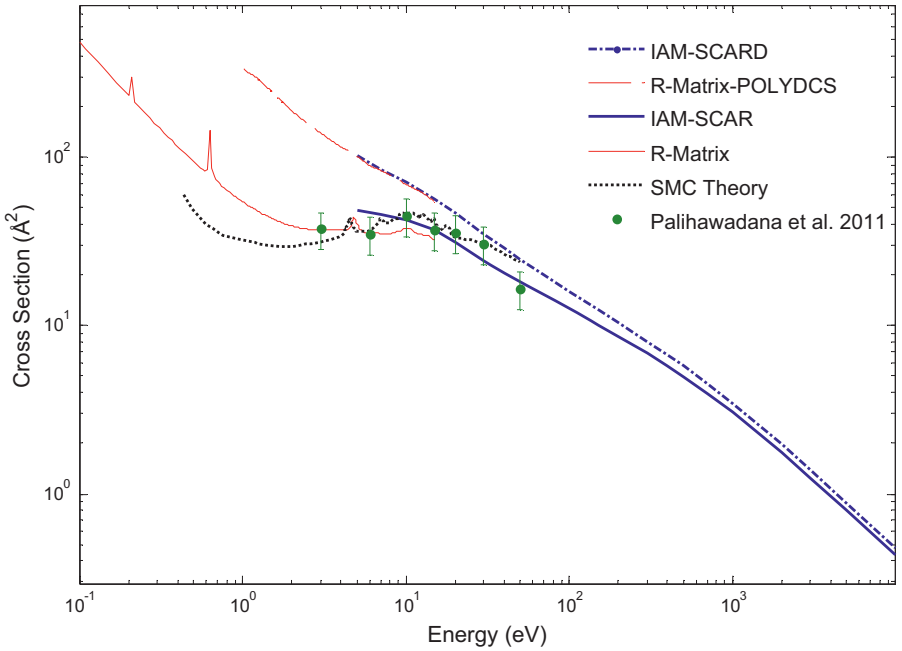

Fig. 4. Theoretical integral cross section for electron scattering by pyrimidine: (solid red line) *R*-matrix elastic cross sections; (solid blue line) IAM-SCAR elastic cross sections; (dashed red line) *R*-matrix-POLYDCS elastic CS plus rotational excitations; (dashed-dotted blue line) IAM-SCARD elastic CS plus rotational excitations; (green asterisk) Palihawadana et al. (2011) experimental data. (For interpretation of the references to colour in this figure legend, the reader is referred to the web version of this article.)

the other hand, the absence of inelastic contributions throughout the single centre expansion approach (ePOLYSCAT) precludes getting realistic cross sections at energies below 10 eV for HCN.

Nonetheless, total cross sections for HCN given by the ePOLYSCAT-POLYDCS procedure (Fig. 5, dashed red line) which comprises the elastic cross sections and rotational excitations are in good agreement with the IAM-SCARD results. For pyrimidine, the *R*-matrix-POLYDCS approach (Fig. 6, dashed red line) provides here reliable TCS up to the ionization potential (9.7 eV) as a sum of elastic scattering, rotational excitations and electronic excitation cross sections. At higher energies, TCS are given by the IAM-SCARD model (Figs. 5 and 6, dashed-dotted blue line) which accounts for the elastic, rotational and electronic excitations, and ionization processes. In spite of inherent limitations at intermediate energies in all the *ab-initio* scattering models we are employing, good

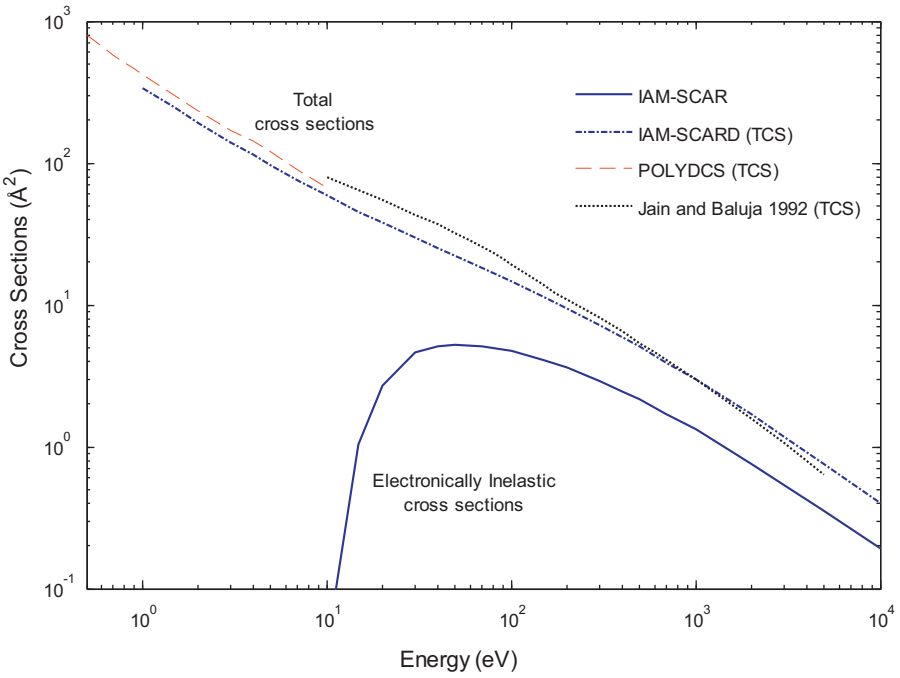

Fig. 5. Computed integral cross section for electron scattering by HCN: (solid blue line) IAM-SCAR electronically inelastic cross sections; (dashed red line) POLYDCS total cross sections; (dashed-dotted blue line) IAM-SCARD total cross sections; (dotted black line) Jain and Baluja (1992). (For interpretation of the references to colour in this figure legend, the reader is referred to the web version of this article.)

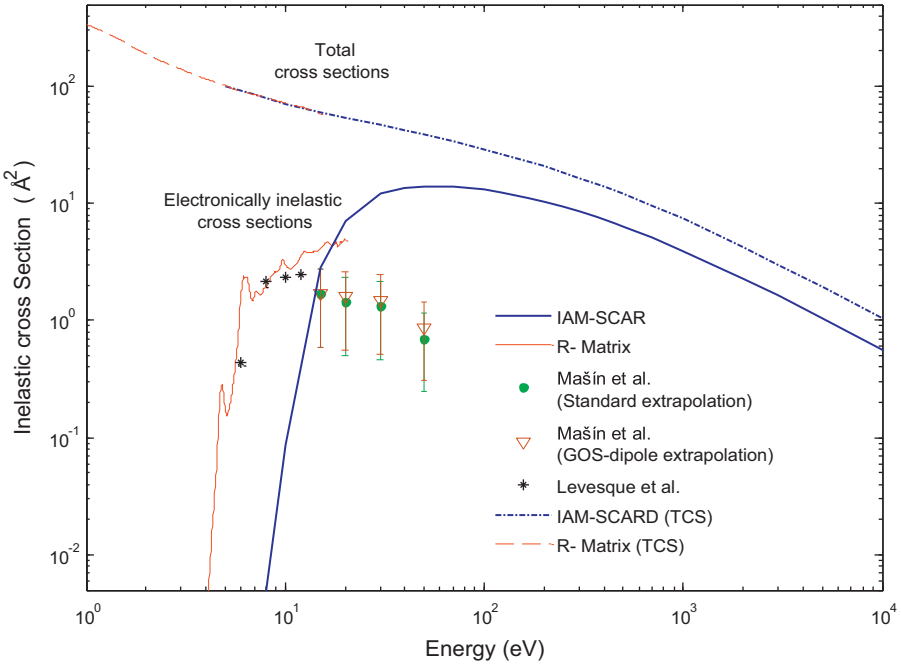

Fig. 6. Computed integral cross section for electron scattering by HCN: (solid red line) *R*-matrix electronically inelastic cross sections; (solid blue line) IAM-SCAR electronically inelastic cross sections; (dashed red line) *R*-matrix total cross sections; (dashed-dotted blue line) IAM-SCARD total cross sections; (black asterisks) Levesque et al. (2005) experimental data; (green dots) Mašín et al. (2012) experimental data with standard extrapolation; (brown triangles) Mašín et al. (2012) experimental data with GOS-extrapolation. (For interpretation of the references to colour in this figure legend, the reader is referred to the web version of this article.)

agreement is achieved across the overlapping energy region both for HCN (Fig. 5) and pyrimidine (Fig. 6).

3.4. *Complete set of integral cross sections*

As a result of the previous discussion, we have generated complete sets of integral cross section data for HCN (Sanz et al., 2012) and pyrimidine (Table 1), chosen as the recommended data from our results. Within the low energy region, from thermalised energies up to the ionization threshold, cross sectional data is reliably provided by either the ePOLYSCAT or the *R*-matrix methods, with the rotational excitations computed by means of the POLYDCS approach. Above the ionization potential, integral cross sections obtained by the IAM-SCAR/SCARD model are favoured. The intrinsic numerical uncertainty for each scattering method is estimated to be around 10% (Muñoz et al., 2007;

Table 1
Electron elastic, rotational, electronically inelastic (electronic excitation and ionization) and total scattering cross sections for pyrimidine from 1 to 10,000 eV.

Energy (eV)	Elastic (Å2)	Rotational (Å2)	Electronic inelastic (Å2)	Total (Å2)
1.0	54.40	281.37		335.77
1.5	43.40	203.60		247.00
2	39.08	149.93		189.00
3	36.84	103.31		140.15
4	36.74	78.94	0.0015	115.68
4.83	43.81	60.66	0.2774	104.74
5	40.48	61.72	0.1722	102.37
7	35.12	48.59	1.61	85.32
10	37.74	31.55	3.02	72.32
15	36.96	19.54	4.04	60.55
20	31.36	15.04	7.17	53.56
30	24.25	10.39	12.12	46.76
40	20.61	7.98	13.64	42.22
50	18.26	6.50	14.03	38.78
70	15.20	4.79	13.92	33.91
100	12.57	3.44	13.08	29.09
150	10.11	2.38	11.56	24.05
200	8.65	1.82	10.30	20.78
300	6.83	1.23	8.51	16.58
400	5.74	0.95	7.25	13.94
500	4.96	0.78	6.36	12.10
700	3.95	0.56	5.10	9.60
1,000	3.05	0.42	3.95	7.42
2,000	1.75	0.21	2.29	4.25
3,000	1.24	0.15	1.63	3.02
5,000	0.80	0.09	1.05	1.93
10,000	0.43	0.05	0.57	1.04

Gianturco and Lucchese, 1998). At intermediate energies, i.e., for the energy region where the different methods are smoothly joined together, we estimate an uncertainty of 20% for HCN (Sanz et al., 2012) whereas we maintain the 10% error for pyrimidine, since *R*-matrix and IAM-SCAR are seen to essentially coincide over that energy range.

4. Present conclusions

Extended computational studies of electron scattering were performed for two different polar molecules, HCN and pyrimidine, over a very broad energy range from low energies (0.1 eV for HCN and 1 eV for pyrimidine) up to 10,000 eV and are reported in this work. Two different *ab-initio* methods were employed in the low energy region: the symmetry adapted-single center expansion model (ePOLYSCAT) and the *R*-matrix method (UKRmol). Both are known to generate reliable elastic cross sections for energies below the ionization potential, whereas the latter (within the close-coupling approximation) also provides electronically inelastic cross sections. For higher energies, above 30 eV, we used the screening-corrected form of the independent-atom model (IAM-SCAR). In order to compare with the experimental data available in the literature, further dipole-induced rotational excitations were computed. The calculated elastic DCS agree very well with prior measurements, both for HCN (Srivastava et al., 1978) and pyrimidine (Maljković et al., 2009; Palihawadana et al., 2011). Although large differences are seen to arise between calculated and experimental integral elastic CS, we found that the reason for this discrepancy is chiefly related to the large contributions to the integral elastic CS coming from the lower angular range of the elastic DCS. The latter range is in general experimentally inaccessible and it is customarily corrected by applying an extrapolation procedure. However, when no extrapolation is applied, we often found that theoretical and experimental integral elastic CS remain in fair agreement.

In conclusion, the present results therefore show that the combination of the quantum scattering methods (ePOLYSCAT and *R*-matrix) at low energies with IAM-SCAR at intermediate and high energies, provides a valid and realistic approach to study electron scattering over a very broad energy range. Even when the target is a strong polar molecule, if one further includes the dipole-induced rotational excitation calculations (POLYDCS and IAM-SCARD), the results are fairly reliable. Although we generally found better agreement between the IAM-SCAR and the *R*-matrix methods at intermediate energies, the lower energy results obtained with the single centre expansion method are consistent with all other findings. It therefore follows that, within this combined approach, complete sets of accurate integral cross sectional data can be generated for molecules of arbitrary properties and geometries, which are in turn essential input for the Monte Carlo track structure simulations and for other biomedical applications.

Acknowledgements

This work is partially supported by the Spanish Ministerio de Economía y Competitividad (Project FIS2009-10245) and the EU/ESF COST Action MP1002 "Nanoscale Insights into Ion Beam Cancer Therapy (Nano-IBCT)". MCF is granted by the Comunidad Autónoma de Madrid local government. This work was also supported by the EPSRC. One of us (FAG) also thanks the Italian MUIR for support through the PRIN 2009–2012 projects.

References

Agostinelli, S., et al., 2003. GEANT4—a simulation tool kit. Nucl. Instrum. Methods Phys. Res., Sect. A 506, 250–303.
Baccarelli, I., Gianturco, F.A., Grandi, A., Sanna, N., 2008. Metastable anion fragmentations after resonant attachment: deoxyribosic structures from quantum electron dynamics. Int. J. Quantum Chem. 108, 1878–1887.
Baró, J., Sempau, J., Fernández-Varea, J.M., Salvat, F., 1995. PENELOPE: an algorithm for Monte Carlo simulation of the penetration and energy loss of electrons and positrons in matter. Nucl. Instrum. Methods Phys. Res., Sect. B 100, 31–46.
Blackman, G.L., Brown, R.D., Burden, F.R., 1970. Microwave spectrum, dipole moment, and nuclear quadrupole coupling constants of pyrimidine. J. Mol. Spectrosc. 35, 444–454.
Blanco, F., García, G., 2002. Improvements on the imaginary part of a non-empirical model potential for electron scattering (30 to 10000 eV energies). Phys. Lett. A 295, 178–184.
Blanco, F., García, G., 2003a. Improvements on the quasifree absorption model for electron scattering. Phys. Rev. A: At. Mol. Opt. Phys. 67, 022701.
Blanco, F., García, G., 2003b. Screening corrections for calculation of electron scattering from polyatomic molecules. Phys. Lett. A 317, 458–462.
Blanco, F., García, G., 2004. Screening corrections for calculation of electron scattering differential cross sections from polyatomic molecules. Phys. Lett. A 330, 230–237.
Burke, P.G., 2011. *R*-Matrix Theory of Atomic Collisions: Application to Atomic Molecular and Optical Processes. Springer.
Burrow, P.D., Howard, A.E., Johnston, A.R., Jordan, K.D., 1992. Temporary anion states of HCN, CH_3CN, $CH_2(CN)_2$, selected cyanoethylenes, benzonitrile, and tetracyanoquinodimethane. J. Phys. Chem. 96, 7570–7578.
Carr, J.M., Galiatsatos, P., Gorfinkiel, J., Harvey, A., Lysaght, M., Madden, D., Mašín, Z., Plummer, M., Tennyson, J., Varambhia, H., 2012. UKRmol: a low-energy electron- and positron-molecule scattering suite. Eur. Phys. J. D 66, 58–69.
Chourou, S.T., Orel, A.E., 2009. Dissociative electron attachment to HCN and HNC. Phys. Rev. A: At. Mol. Opt. Phys. 80, 032709.
Collins, L.A., Norcross, D.,W., 1978. Electron collisions with highly polar-molecules—comparison of model, static, and static-exchange calculations for alkali-metal halides. Phys. Rev. A: At. Mol. Opt. Phys. 18, 467–498.
Cowan, R.D., 1981. The Theory of Atomic Structure and Spectra. University of California Press, London.
Crawford, O.H., 1967. Scattering of low-energy electrons from polar molecules. J. Chem. Phys. 47, 1100–1104.
DeLeon, R.L., Muenter, J.S., 1984. The vibrational dipole-moment function of HCN. J. Chem. Phys. 80, 3992–3999.
DeVoe, H., Tinoco Jr., I., 1962. Stability of helical polynucleotides—base contributions. J. Mol. Biol. 4, 500–517.

Dickinson, A.S., 1977. Differential cross sections for electron scattering by strongly polar molecules. J. Phys. B: At. Mol. Opt. Phys. 10, 967–981.
Faure, A., Gorfinkiel, J.D., Morgan, L., Tennyson J., A., 2002. GTOBAS: fitting continuum functions with Gaussian-type orbitals. Comput. Phys. Commun. 144, 224–241.
Faure, A., Varambhia, H.N., Stoecklin, T., Tennyson, J., 2007. Electron-impact rotational and hyperfine excitation of HCN, HNC, DCN and DNC. Mon. Not. R. Astron. Soc. 382, 840–852.
Ferreira da Silva, F., Almeida, D., Martins, G., Milosavljevic, A.R., Marinkovic, B.P., Hoffmann, S.V., Mason, N.J., Nunes, Y., García, G., Limão-Vieira, P., 2010. The electronic states of pyrimidine studied by VUV photoabsorption and electron energy-loss spectroscopy. Phys. Chem. Chem. Phys. 12, 6717.
Fischer, G., Cai, Z.L., Reimers, J.R., Wormell, P., 2003. Singlet and triplet valence excited states of pyrimidine. J. Phys. Chem. A 107, 3093.
Frisch, M.J., Trucks, G.W., Schlegel, H.B. et al., 2004. Gaussian 03 (Wallingford, CT: Gaussian Inc., revision c.02).
Fuller, D.B., Koziol, J.A., Feng, A.C., 2004. Prostate brachytherapy seed migration and dosimetry: analysis of stranded sources and other potential predictive factors. Brachytherapy 3, 10–19.
Gemmel, A., Hasch, B., Ellerbrock, M., Weyrather, W.K., Krämer, M., 2008. Biological dose optimization with multiple ion fields. Phys. Med. Biol. 53, 6991–7012.
Gianturco, F.A., Lucchese, R.R., 1998. One-electron resonances and computed cross sections in electron scattering from the benzene molecule. J. Chem. Phys. 108, 6144–6159.
Gianturco, F.A., Lucchese, R.R., 2004. Resonant capture of low-energy electrons by gas-phase glycine: a quantum dynamics calculation. J. Phys. Chem. A 108, 7056–7062.
Gianturco, F.A., Lucchese, R.R., Sanna, N., 1994. Calculation of low-energy elastic cross-sections for electron-CF4 scattering. J. Chem. Phys. 100, 6464–6471.
Hara, S.J., 1967. Scattering of slow electrons by hydrogen molecules. J. Phys. Soc. Jpn. 22, 710–718.
Herzberg, G., 1966. Electronic Spectra and Electronic Structures of Polyatomic Molecules (Van Nostrand, New York).
Hush, N., Cheung, A.S., 1975. Ionization potentials and donor properties of nucleic acid bases and related compounds. Chem. Phys. Lett. 34, 11–13.
Jain, A., 1988. Theoretical study of the total (elastic plus inelastic) cross sections for electron—H_2O (NH_3) scattering at 10–3000 eV. J. Phys. B: At. Mol. Opt. Phys. 21, 905–924.
Jain, A., Baluja, K.L., 1992. Total (elastic plus inelastic) cross-sections for electron-scattering from diatomic and polyatomic-molecules at 10–5000 eV: H_2, Li_2, HF, CH_4, N_2, CO, C_2H_2, HCN, O_2, HCl, H_2S, PH_3, SiH_4, and CO_2. Phys. Rev. A: At. Mol. Opt. Phys. 45, 202–218.
Jain, A., Norcross, D.W., 1985. Ab initio calculations of low-energy electron scattering by HCN molecules. Phys. Rev. A: At. Mol. Opt. Phys. 32, 134–143.
Kato, H., Suga, A., Hoshino, M., Blanco, F., García, G., Limão-Vieira, P., Brunger, M.J., Tanaka, H., 2012. Elastic cross sections for electron scattering from GeF_4: predominance of atomic-F in the high-energy collision dynamics. J. Chem. Phys. 136, 134313.
Kulakowski, I., Geller, M., Lesyng, B., Wierzcho, K.L., 1974. Dipole-moments of 2,4-diketopyrimidines. 2. Uracil, thymine and their derivatives. Biochim. Biophys. Acta 361, 119–130.
Lane, N.F., 1980. Theory of electron–molecule collisions. Rev. Mod. Phys. 59, 29–119.
Lee, C., Yang, W., Parr, R.G., 1998. Development of the Colle–Salvetti correlation-energy formula into a functional of the electron density. Phys. Rev. B: Condens. Matter 37, 785–789.
Levesque, P.L., Michaud, M., Sanche, L., 2005. Absolute vibrational and electronic cross sections for low-energy electron (2–12 eV) scattering from condensed pyrimidine. J. Chem. Phys. 122, 094701.
Limão-Vieira, P., Blanco, F., Oller, J.C., Muñoz, A., Pérez, J.M., Vinodkumar, M., García, G., Mason, N., 2005. Electron scattering cross sections for SF6 and SF5CF3 at intermediate and high energies.100–10,000 eV. J. Phys. Rev. A 71, 032720.
Limão-Vieira, P., Horie, M.H., Kato, Hoshino, M., Blanco, F., García, G., Buckman, S.J., Tanaka, H., 2011. Differential elastic electron scattering cross sections for CCl_4 by 1.5–100 eV energy electron impact. J. Chem. Phys. 135, 234309.
Lucchese, R.R, Gianturco, F.A., 1996. One-electron resonances in electron scattering from polyatomic molecules. Int. Rev. Phys. Chem. 15, 429–466.
Maljković, J.B., Milosavljević, A.R., Blanco, F., Šević, D., García, G., Marinković, B.P., 2009. Absolute differential cross sections for elastic scattering of electrons from pyrimidine. Phys. Rev. A: At. Mol. Opt. Phys. 79, 052706.
Märk, T. D., Hatano, Y., Linder, F., 1995. Electron Collision Cross Sections; IAEA-TECDOC-799; International Atomic Energy Agency (IAEA): Vienna, Austria, pp. 163–275.
Mašín, Z., Gorfinkiel, J.D., 2011. Elastic and inelastic low-energy electron collisions with pyrazine. J. Chem. Phys. 135, 144308.
Mašín, Z., Gorfinkiel, J.D., Jones, D.B., Bellm, S.M., Brunger, M.J., 2012. Elastic and inelastic cross sections for low-energy electron collisions with pyrimidine. J. Chem. Phys. 136, 144310.
May, O., Kubala, D., Allan, M., 2010. Absolute cross sections for dissociative electron attachment to HCN and DCN. Phys. Rev. A: At. Mol. Opt. Phys. 82, 010701.
Muñoz, A., Oller, J.C., Blanco, F., Gorfinkiel, J., Limão-Vieira, P., García, G., 2007. Electron-scattering cross sections and stopping powers in H_2O. Phys. Rev. A: At. Mol. Opt. Phys. 76, 052707.
Natalense, A.P.P., Lucchese, R.R., 1999. Cross section and asymmetry parameter calculation for sulfur 1s photoionization of SF6. J. Chem. Phys. 111, 5344–5348.
Nayak, A.K., Chaudhuri, R.K., Krishnamachari, S.N.L.G., 2005. Theoretical study on the excited states of HCN. J. Chem. Phys. 122, 184323.
Nelson Jr., R.D., Lide, D.R., Maryott, A.A., 1967. Selected Values of Electric Dipole Moments for Molecules in the Gas Phase, NSRDS-NBS Series, vol. 10. US GPO, Washington, DC.
Norcross, D.W., Collins, L.A., 1982. Recent developments in the theory of electron-scattering by highly polar-molecules. Adv. At. Mol. Phys. 18, 341–397.
Okamoto, Y., Onda, K., Itikawa, Y., 1993. Vibrationally elastic cross sections for electron scattering from water molecules. J. Phys. B: At. Mol. Opt. Phys. 26, 745–758.
Palihawadana, P., Sullivan, J.P, Brunger, M.J., Winstead, C., McKoy, V., García, G., Blanco, F., Buckman, S.J., 2011. Low-energy elastic electron interactions with pyrimidine. Phys. Rev. A: At. Mol. Opt. Phys. 84, 062702.
Pimblott, S.M., LaVerne, J.A., 2007. Production of low-energy electrons by ionizing radiation. Radiat. Phys. Chem. 76, 1244–1247.
Riley, M.E., Truhlar, D.G., 1975. Approximations for the exchange potential in electron scattering. J. Chem. Phys. 63, 2182–2192.
Sanna, N., Gianturco, F.A., 1998. Differential cross sections for electron/positron scattering from polyatomic molecules. Comput. Phys. Commun. 114, 142–167.
Sanz, A.G., Fuss, M.C., Blanco, F., Sebastianelli, F., Gianturco, F.A., García, G., 2012. Electron scattering cross sections from HCN over a broad energy range (0.1–10000 eV): influence of the permanent dipole moment on the scattering process. J. Chem. Phys. 137, 124103.
Schreiber, M., Silva-Junior, M.R., Sauer, S.P.A., Thiel, W., 2008. Benchmarks for electronically excited states: CASPT2, CC2, CCSD, and CC3. J. Chem. Phys. 128, 134110.
Srivastava, S.K., Tanaka, H., Chutjian, A., 1978. Elastic scattering of intermediate energy electrons by HCN. J. Chem. Phys. 69, 1493–1497.
Staszewska, G., Schwenke, D.W., Thirumalai, D., Truhlar, D.G., 1983. Quasifree-scattering model for the imaginary part of the optical potential for electron scattering. Phys. Rev. A: At. Mol. Opt. Phys. 28, 2740–2751.
Suresh, S.J., Naik, V.M., 2000. Hydrogen bond thermodynamic properties of water from dielectric constant data. J. Chem. Phys. 113, 9727–9732.
Tennyson, J., 2010. Electron-molecule collision calculations using the *R*-matrix method. Phys. Rep. 491, 29–76.
Varambhia, H.N., Tennyson, J., 2007. Electron collision with the HCN and HNC molecules using the *R*-matrix method. J. Phys. B: At. Mol. Opt. Phys. 40, 1211–1223.
Weber, H.P., Craven, B.M., 1990. Electrostatic properties of cytosine monohydrate from diffraction data. Acta Crystallogr., Sect. B: Struct. Sci 46, 532–538.
Werner, H.J., Knowles, P. J., Lindh, R., Manby, F.R., Schütz, M., et al., 2009. MOLPRO, version 2009.1, a package of *ab initio* programs, see 〈http://www.molpro.net〉.
Zatsarinny, O., Bartschat, K., García, G., Blanco, F., Hargreaves, L.R., Jones, D.B., Murrie, R., Brunton, J.R., Brunger, M.J., Hoshino, M., Buckman, S.J., 2011. Electron-collision cross sections for iodine. Phys. Rev. A: At. Mol. Opt. Phys. 83, 042702.
Zecca, A., Chiari, L., García, G., Blanco, F., Trainotti, E., Brunger, M.J., 2011. Total cross-sections for positron and electron scattering from α-tetrahydrofurfuryl alcohol. New J. Phys. 13, 063019.
Zhang, R., Faure, A., Tennyson, J., 2009. Electron and positron collisions with polar molecules: studies with the benchmark water molecule. Phys. Scr. 80, 015301.
Zhang, X.Z., Sun, J.F., Liu, Y.F., 1992. A new approach to the correlation polarization potential-low-energy electron elastic scattering by He atoms. J. Phys. B: At. Mol. Opt. Phys. 25, 1893–1897.